Functional differences in Na^+ channel gating between fast-spiking interneurones and principal neurones of rat hippocampus

Marco Martina and Peter Jonas*

Physiologisches Institut der Universität Freiburg, D-79104 Freiburg, Germany

1. GABAergic interneurones differ from glutamatergic principal neurones in their ability to discharge high-frequency trains of action potentials without adaptation. To examine whether Na^+ channel gating contributed to these differences, Na^+ currents were recorded in nucleated patches from interneurones (dentate gyrus basket cells, BCs) and principal neurones (CA1 pyramidal cells, PCs) of rat hippocampal slices.

2. The voltage dependence of Na^+ channel activation in BCs and PCs was similar. The slope factors of the activation curves, fitted with Boltzmann functions raised to the third power, were 11·5 and 11·8 mV, and the mid-point potentials were −25·1 and −23·9 mV, respectively.

3. Whereas the time course of Na^+ channel activation (−30 to +40 mV) was similar, the deactivation kinetics (−100 to −40 mV) were faster in BCs than in PCs (tail current decay time constants, 0·13 and 0·20 ms, respectively, at −40 mV).

4. Na^+ channels in BCs and PCs differed in the voltage dependence of inactivation. The slope factors of the steady-state inactivation curves fitted with Boltzmann functions were 6·7 and 10·7 mV, and the mid-point potentials were −58·3 and −62·9 mV, respectively.

5. The onset of Na^+ channel inactivation at −55 mV was slower in BCs than in PCs; the inactivation time constants were 18·6 and 9·3 ms, respectively. At more positive potentials the differences in inactivation onset were smaller.

6. The time course of recovery of Na^+ channels from inactivation induced by a 30 ms pulse was fast and mono-exponential ($\tau = 2{\cdot}0$ ms at −120 mV) in BCs, whereas it was slower and bi-exponential in PCs ($\tau_1 = 2{\cdot}0$ ms and $\tau_2 = 133$ ms; amplitude contribution of the slow component, 15%).

7. We conclude that Na^+ channels of BCs and PCs differ in gating properties that contribute to the characteristic action potential patterns of the two types of neurones.

Cortical neurones differ markedly in their intrinsic action potential patterns (reviewed by Connors & Gutnick, 1990). Glutamatergic principal neurones in the hippocampus and neocortex are either regularly spiking or intrinsically bursting and show adaptation during sustained current injection (Madison & Nicoll, 1984; Stafstrom, Schwindt & Crill, 1984). In contrast, several types of GABAergic interneurones are fast spiking and generate trains of several hundred action potentials per second without any adaptation (McCormick, Connors, Lighthall & Prince, 1985; Lacaille & Williams, 1990; Han, Buhl, Lörinczi & Somogyi, 1993). This diversity in the intrinsic firing patterns of neurones is of critical importance for the operation of the entire neuronal network, because it shapes the transformation of synaptic input signals into action potential output signals.

The determinants of this heterogeneity in intrinsic firing patterns of cortical neurones are not entirely understood. The basic functional properties of voltage-gated Na^+ channels expressed in principal neurones have been studied (Sah, Gibb & Gage, 1988; Fleidervish, Friedman & Gutnick, 1996), but those of Na^+ channels in fast-spiking interneurones have not been investigated. Previous studies indicated that voltage-gated K^+ channels expressed in principal neurones and interneurones differ in their functional properties (Storm, 1990; Zhang & McBain, 1995*a*, *b*). K^+ channels in interneurones activate and deactivate rapidly, but inactivate only very slowly (Zhang & McBain, 1995*a*, *b*); these gating properties will support the sustained generation of action potentials with high frequency in interneurones. In addition, both the distribution of the different channels and the

* To whom correspondence should be addressed.

structure of the dendritic tree influence the discharge pattern of cortical neurones (Mainen & Sejnowski, 1996).

To explore the possibility that specific characteristics of Na^+ channel gating contribute to the differences in spiking patterns, we compared Na^+ channels of a fast-spiking GABAergic interneurone (the dentate gyrus basket cell) with those of a regularly spiking or bursting principal neurone (the CA1 pyramidal cell). Analysis of the very rapid gating of Na^+ channels requires adequate voltage-clamp control of the neuronal membrane; we have therefore used the nucleated patch technique (Sather, Dieudonné, MacDonald & Ascher, 1992; Terlau, Shon, Grilley, Stocker, Stühmer & Olivera, 1996) to record macroscopic Na^+ currents under almost ideal voltage-clamp conditions. Our results show that Na^+ channels in the two cell types differ in their functional properties, particularly regarding the inactivation process. These differences contribute to the characteristic action potential patterns of the two classes of neurones.

METHODS

Cell identification and isolation of nucleated patches

Nine- to 16-day-old Wistar rats were killed by decapitation (according to local regulations). Transverse 300 μm thick hippocampal slices were cut from the brains using a vibratome (Dosaka, Kyoto, Japan). Basket cells in the dentate gyrus (BCs) and pyramidal neurones in the CA1 subfield (PCs) were identified visually using infrared differential interference contrast (IR-DIC) videomicroscopy (Stuart, Dodt & Sakmann, 1993) and on the basis of their characteristic action potential pattern following sustained current injection (Lacaille & Williams, 1990; Han *et al.* 1993). Patch pipettes were pulled from borosilicate glass tubing (2·0 mm outer diameter, 0·5 mm wall thickness; Hilgenberg, Malsfeld, Germany), coated with Sylgard (184; Dow Corning), and heat polished directly before use. Neurones were approached with patch pipettes under visual control; positive pressure was applied to the pipette during this procedure (Stuart *et al.* 1993). Following seal formation, access to the cell interior was obtained by applying a brief pulse of suction. The resistance of patch pipettes (when filled with internal solution) ranged from 2 to 5 MΩ, and the series resistance in the whole-cell configuration ranged from 4 to 15 MΩ. Only neurones with initial resting potentials negative to −55 mV were used. The action potential pattern of BCs was tested within 10 s after obtaining access to the cell interior. To isolate nucleated patches (Sather *et al.* 1992), negative pressure (5–15 kPa) was applied and the patch pipette was withdrawn slowly. The input resistance of the nucleated patches ranged from 2 to 5 GΩ. Their shape was spherical, and the diameter was 3·5–5·0 μm, corresponding to a surface membrane area of 38·5–78·5 μm^2.

Recording of Na^+ currents

Patch currents were recorded using an Axopatch 200A amplifier (Axon Instruments, Foster City, CA, USA). Signals were filtered at 10 kHz (or 50 kHz for deactivation) using the built-in 4-pole low-pass Bessel filter. Capacitive transients were minimized by maintaining the bath at the lowest possible level, and were further reduced by the capacitive compensation circuit of the amplifier. As the mean peak amplitude of the Na^+ currents at 0 mV was only 202 ± 27 pA for BCs and 179 ± 12 pA for PCs, series resistance compensation was not used. A CED 1401plus interface (CED, Cambridge, UK) connected to a personal computer was used for stimulus generation and data acquisition. The sampling frequency was 20 or 40 kHz. In some experiments, the voltage pulses were low-pass filtered prior to the amplifier input (filter time constant, 5 μs) to reduce the amplitude of the capacitive transients.

We estimate that, in the worst case (series resistance (R) = 15 MΩ, membrane area (A) = 78·5 μm^2), the membrane of a nucleated patch follows a command voltage step with an overall time constant of approximately 13 μs, composed of: (1) the time constant of the resistance–capacitance equivalent circuit ($\tau = RC_mA = 8$ μs), where C_m is the specific membrane capacitance (0·7 $\mu F\ cm^{-2}$), and (2) the time constant of the filter at the amplifier input, 5 μs. Further distortion of the signals arises from residual capacitive components and from the effect of the filter at the amplifier output (10–90% rise time: 7 or 34 μs, depending on the filter setting; Colquhoun & Sigworth, 1995). Considering these factors, sample points 25–100 μs following a voltage step were excluded from the fitting of the time course and were blanked in the figures.

Nucleated patches were held at −90 mV. A 50 ms pulse to −120 mV was applied before each test pulse to obtain complete recovery from fast inactivation. K^+ channels were blocked by external TEA^+ and internal Cs^+. Ca^{2+} channels appeared to be largely absent from nucleated patches, because 100 μM external Cd^{2+} did not have any effect on the recorded currents. Leakage and capacitive currents were subtracted on-line using a $P/-4$ protocol (four negative correction pulses, amplitude 1/4 of that of the test pulse). Alternatively, Na^+ currents were isolated by off-line subtraction of currents recorded in the absence from those recorded in the presence of 1 μM external tetrodotoxin (TTX; Sigma). TTX subtraction was performed in the majority of experiments; it was done for all pulse protocols with test pulses to potentials ⩾ +10 mV (at these potentials a residual outward current resistant to external TEA^+ and Cd^{2+} and internal Cs^+ appeared). Traces in the figures were TTX subtracted and filtered digitally (Gaussian characteristics, 3 or 5 kHz); they represent single sweeps or averages of up to eighteen sweeps. Test pulses were applied every 4–5 s. During the course of the experiments, the Na^+ current amplitude was stable within ±20% of the initial value, otherwise the patch was discarded. No correction for liquid junction potentials (approximately 4 mV) was made. All recordings were performed at room temperature (22–24 °C). The data included in this study were obtained from 121 nucleated patches (47 BC patches, 74 PC patches).

Solutions and chemicals

Slices were continuously superfused with physiological extracellular solution containing (mM): 125 NaCl, 25 $NaHCO_3$, 2·5 KCl, 1·25 NaH_2PO_4, 2 $CaCl_2$, 1 $MgCl_2$, 25 glucose, bubbled with 95% O_2 and 5% CO_2. Tetraethylammonium chloride (20 mM; TEA; Merck) and, in some experiments, 100 μM $CdCl_2$ were added to the bath solution to block voltage-gated K^+ channels and Ca^{2+} channels, respectively. Pipettes were filled with Cs^+-rich internal solution, containing (mM): 140 CsCl, 10 EGTA, 2 $MgCl_2$, 2 Na_2ATP, 10 Hepes, pH adjusted to 7·3 with CsOH. In some experiments 2 mM TEA was added to the internal solution. In experiments designed to measure the reversal potentials of the Na^+ currents, internal solutions containing 132 mM CsCl plus 8 mM NaCl, or 60 mM CsCl plus 80 mM NaCl (Fig. 1) were used. All chemicals were from Merck or Sigma.

Analysis

The time courses of deactivation, onset of inactivation, and recovery from inactivation were fitted either with a single exponential or with the sum of two exponentials, using a non-linear

least-squares algorithm. The activation time constant was determined by fitting Na^+ currents (range, 0–4·5 ms) with the function:

$$f = \{1 - \exp[-(t - \delta t)/\tau_m]\}^3 \exp(-t/\tau_h) \text{ for } t > \delta t,\ f = 0 \text{ for } t \leqslant \delta t,$$

where t is time, δt is a delay, τ_m is the activation time constant, and τ_h the inactivation time constant (see Jonas, 1989). The activation curve was obtained from the peak current–voltage relation using the Goldman–Hodgkin–Katz equation (Hille, 1992) and was fitted with a Boltzmann function raised to the third power:

$$f = 1/\{1 + \exp[-(V - V_{½})/k]\}^3,$$

where V is membrane potential, $V_{½}$ is the potential at which the value of the Boltzmann function is 0·5, and k is the slope factor. The steady-state inactivation (h_∞) curve was fitted with a simple Boltzmann function:

$$f = 1/\{1 + \exp[(V - V_{½})/k]\}.$$

All numerical values given denote means ± S.E.M. Error bars in figures (representing S.E.M.) were plotted only when they exceeded the respective symbol size. The data points shown in the figures and the mean values given in the text and Table 1 were obtained by pooling data from different patches. Individual experiments were also analysed separately to test statistical significance and to obtain the standard errors; when these results were averaged, the mean values were very similar to the results obtained by fitting the pooled data. Statistical significance was assessed using Student's t test (unpaired samples, two-sided) at the significance level (P) indicated.

RESULTS

Voltage dependence of Na^+ channel activation

To address whether differences in Na^+ channel gating contributed to the marked differences in spiking pattern between dentate gyrus basket cells and CA1 pyramidal neurones of rat hippocampus, we examined Na^+ currents in the two classes of cells using the nucleated patch configuration. The voltage dependence of Na^+ channel activation was studied using test pulses to membrane potentials between −80 and +40 mV (Fig. 1).

Representative recordings of Na^+ currents with 84 mM internal Na^+ are shown in Fig. 1*A* and *B*. Under these conditions, the amplitude of the Na^+ inward current was maximal at approximately −20 mV in both types of neurones. At more positive voltages, the Na^+ currents became smaller and finally reversed; the interpolated reversal potentials were +15·6 ± 1·4 mV in BC patches ($n = 3$) and +15·0 ± 0·5 mV in PC patches ($n = 4$). With 12 and 4 mM

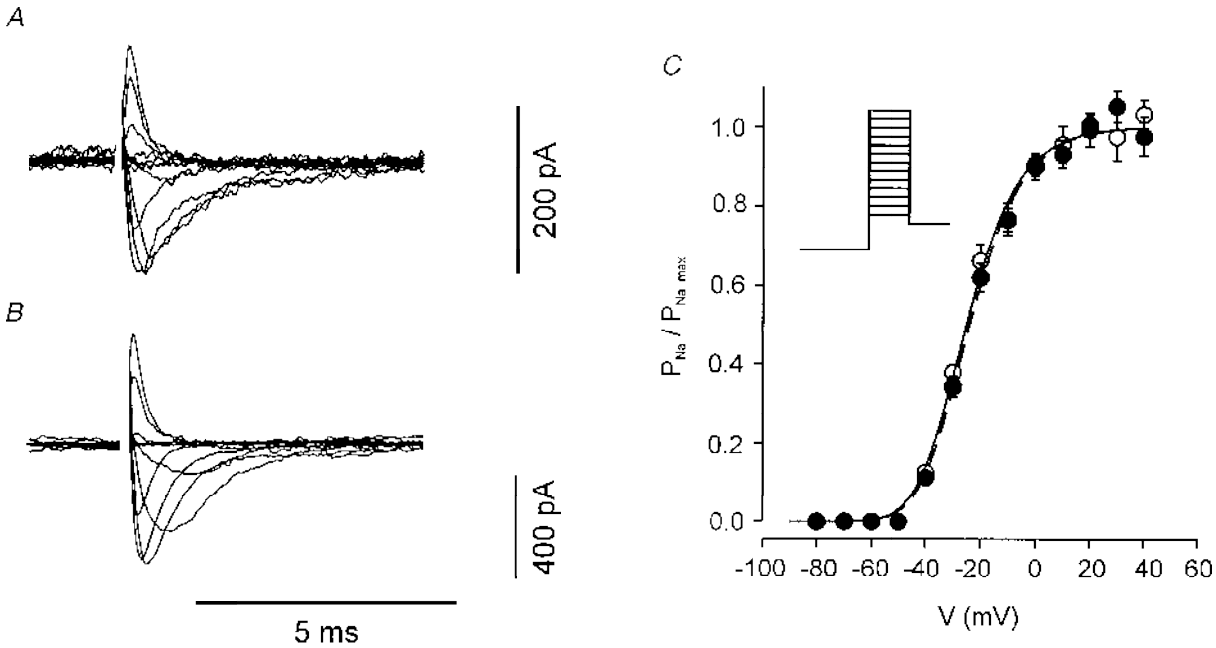

Figure 1. Voltage dependence of activation of Na^+ channels in BC and PC patches

A and *B*, traces of Na^+ current recorded from a BC nucleated patch (*A*) and a PC nucleated patch (*B*) at different test pulse potentials. Pulse protocol: holding potential, −90 mV; 50 ms pulse to −120 mV; 30 ms test pulse to membrane potentials between −80 and +40 mV (10 mV increments); and step back to −90 mV (see inset in *C*). The internal solution was Cs^+-rich solution containing 84 mM Na^+. *C*, Na^+ permeability (P_{Na}), normalized to the maximal value, was plotted against test pulse potential. Permeability values were calculated from the respective Na^+ peak current amplitudes using the Goldman–Hodgkin–Katz equation (Hille, 1992). Open circles and continuous curve: mean values from 8 BC nucleated patches (5 patches with 4 mM and 3 patches with 84 mM internal Na^+). Filled circles and dashed curve: mean values from 13 PC nucleated patches (9 patches with 4 mM and 4 patches with 84 mM internal Na^+). Curves represent Boltzmann functions raised to the third power fitted to the data points; for curve parameters, see Table 1.

internal Na^+, the reversal potentials obtained by linear extrapolation were more positive, +63·6 ± 4 mV and +70·0 ± 4·3 mV in BC patches ($n = 7$) and +60·6 ± 5·5 mV and +75·1 ± 4·0 mV in PC patches ($n = 9$), respectively. These results were consistent with the predictions of the Nernst equation for a Na^+-selective channel.

To obtain Na^+ channel activation curves, the Na^+ permeability at a given test pulse potential was calculated

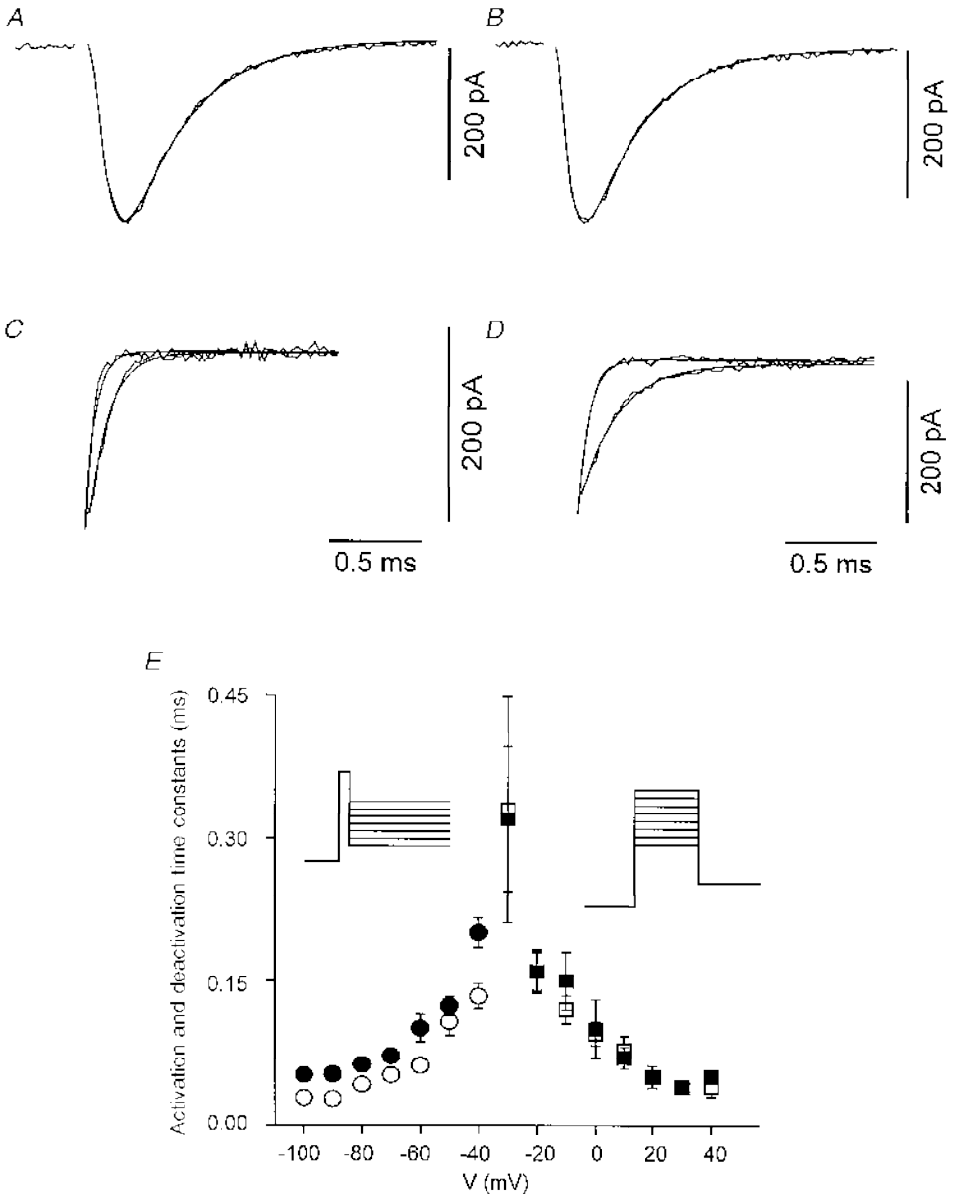

Figure 2. Time course of activation and deactivation of Na^+ channels in BC and PC patches

A and *B*, time course of activation of Na^+ channels in a BC nucleated patch (*A*) and a PC nucleated patch (*B*) at 0 mV. Pulse protocol as in Fig. 1, test pulse potential, 0 mV (see right inset in *E*). The rising and early decay phases of the current were fitted with the function: $f = \{1 - \exp[-(t - \delta t)/\tau_m]\}^3 \exp(-t/\tau_h)$ for $t > \delta t$, $f = 0$ for $t \leqslant \delta t$, where τ_m and τ_h denote the activation and inactivation time constant, respectively. The respective curves are shown superimposed. *C* and *D*, time course of deactivation of Na^+ channels in a BC nucleated patch (*C*) and a PC nucleated patch (*D*) at −90 and −50 mV. Pulse protocol: holding potential, −90 mV; 50 ms pulse to −120 mV; 300 μs pulse to 0 mV; 50 ms test pulse to −90 mV or −50 mV; and step back to −90 mV (see left inset in *E*). The decay of the tail current following the brief pulse was fitted with an exponential function; the respective curves are shown superimposed. The internal solution in *A*–*D* was Cs^+-rich solution containing 4 mM Na^+. *E*, activation (squares) and deactivation (tail current decay; circles) time constants plotted against test pulse potential. Open symbols: mean values from 6 and 5 BC nucleated patches, respectively. Filled symbols: mean values from 8 and 6 PC nucleated patches, respectively.

Table 1. Comparison of functional properties of Na^+ channels in interneurones and pyramidal neurones of the hippocampus

Parameter	Basket cells	Pyramidal cells	Significance
Activation curve mid-point potential (mV)	−25·1 ± 0·9 (8)	−23·9 ± 0·9 (13)	—
k (mV)	11·5 ± 0·7 (8)	11·8 ± 0·8 (13)	—
Activation τ (−20 mV) (ms)	0·16 ± 0·02 (6)	0·16 ± 0·02 (8)	—
Deactivation τ (−40 mV) (ms)	0·13 ± 0·01 (5)	0·20 ± 0·02 (6)	$P < 0·01$
Inactivation curve mid-point potential (mV)	−58·3 ± 0·8 (11)	−62·9 ± 1·7 (17)	$P < 0·05$
k (mV)	6·7 ± 0·5 (11)	10·7 ± 0·9 (17)	$P < 0·005$
Onset of inactivation τ (−20 mV) (ms)	1·34 ± 0·14 (16)	0·84 ± 0·01 (19)	$P < 0·01$
Onset of inactivation τ (−55 mV) (ms)	18·6 ± 4·2 (6)	9·3 ± 1·0 (7)	$P < 0·05$
Recovery from inactivation τ (ms)	2·0 ± 0·4 (13)	2·0 ± 0·2 (85 ± 1 %) (8–14)	—
(30 ms conditioning pulse)		133 ± 24 (15 ± 1 %) (8–14)	$P < 0·001$
Recovery from inactivation τ (ms)	2·7 ± 0·1 (3)	2·6 ± 0·2 (76 ± 2 %) (4–7)	—
(300 ms conditioning pulse)		351 ± 34 (24 ± 2 %) (4–7)	$P < 0·001$
I_9/I_1 (multiple pulses) (%)	94 ± 5 (5)	67 ± 4 (5)	$P < 0·005$

Values indicate means ± S.E.M., and total number of nucleated patches (in parentheses). The values given in parentheses for the time constants of recovery from inactivation in PCs indicate the amplitude contribution of each component (expressed as a percentage). Significance of differences in the time course of recovery from inactivation were assessed by comparing the fraction of the current that recovered within 11 ms at −120 mV in the two classes of cells. I_9/I_1 denotes the ratio of Na^+ currents evoked by the last and the first pulse in a train; 9 pulses to 0 mV (30 ms duration) separated by pulses to −120 mV (12 ms duration).

from the respective peak current amplitude using the Goldman–Hodgkin–Katz equation (Hille, 1992). Permeability was then normalized to the maximal value and plotted against test pulse potential (Fig. 1*C*). The activation curves for BC and PC patches were similar, and fits with Boltzmann functions raised to the third power gave almost identical values for both the mid-point potentials (−25·1 ± 0·9 and −23·9 ± 0·9 mV, respectively; $P > 0·2$) and the slope factors (11·5 ± 0·7 and 11·8 ± 0·8 mV; $n = 8$ and 13, respectively; $P > 0·5$; Fig. 1*C* and Table 1). These results indicate that the voltage dependence of activation of Na^+ channels expressed in BCs and PCs was similar.

Time course of activation and deactivation

The time course of activation of Na^+ channels was investigated using test pulses to potentials ranging from −30 to +40 mV. In both BC and PC patches, the rise of the Na^+ current was sigmoidal, and could be well fitted with an exponential function raised to the third power and shifted with respect to the onset of the pulse by a small delay (Fig. 2*A* and *B*). The time constants of activation became smaller with increasing voltage, and their values were similar for the two types of neurones over the range of membrane potentials tested (Fig. 2*E*). The activation time constant at −20 mV, for instance, was 0·16 ± 0·020 ms for BC patches ($n = 6$) and 0·16 ± 0·023 ms for PC patches ($n = 8$; $P > 0·5$).

The time course of deactivation of Na^+ channels was investigated using a 300 μs pulse to 0 mV followed by a step to potentials between −100 and −40 mV. Analysis of tail currents following the brief pulses (Fig. 2*C* and *D*) indicated that the time course of Na^+ channel deactivation differed between the two types of neurones (Fig. 2*E*). The value of the deactivation time constant at −40 mV, for example, was 0·134 ± 0·013 ms ($n = 5$) in BC patches, whereas it was significantly larger (0·201 ± 0·015 ms, $n = 6$; $P < 0·01$) in PC patches. On average, the deactivation time constant of PC Na^+ channels was 1·57-fold larger than that of BC Na^+ channels ($P < 0·05$ for 5 out of 7 potentials). These results indicate that Na^+ channels expressed in BCs deactivate more rapidly than those expressed in PCs.

Steady-state inactivation curve

A marked difference between BC and PC Na^+ channels was observed in the voltage dependence of steady-state inactivation (h_∞), measured using prepulses to membrane potentials between −120 and −30 mV (Fig. 3). In both types of neurones the inactivation curves were well described by Boltzmann functions. The mid-point potential of the inactivation curve was −58·3 ± 0·8 mV in BC patches ($n = 11$), whereas it was more negative (−62·9 ± 1·7 mV) in PC patches ($n = 17$; $P < 0·05$). The slope factor of the inactivation curve was significantly different between the two classes of cells; the mean value was 6·7 ± 0·5 mV in BC patches, whereas it was 1·6-fold larger (10·7 ± 0·9 mV) in PC patches ($P < 0·005$; Fig. 3*C* and Table 1). These results show that the voltage dependence of the inactivation process is significantly steeper for BC Na^+ channels than for PC Na^+ channels.

Time course of onset of inactivation

Na^+ channels expressed in BCs and PCs also differed in the kinetics of inactivation onset during test pulses to potentials between −30 and +40 mV (Fig. 4). The time course of inactivation onset was mono-exponential in almost all BC patches (16 out of 16 at −20 mV) and in the majority of PC patches (14 out of 21 at −20 mV; see Howe & Ritchie, 1992). In five PC patches, however, the inactivation onset was slightly better fitted with the sum of two exponentials at some voltages, and in two PC patches it was clearly bi-exponential at all potentials. These two PC patches were not included in the analysis of inactivation kinetics.

The inactivation time constants decreased with increasing membrane potential in both BCs and PCs, but their values differed between the two classes of neurones (Fig. 4*C*). The inactivation time constant at −20 mV, for example, was 1·34 ± 0·14 ms in BC patches ($n = 16$) and 0·84 ± 0·01 ms in PC patches ($n = 19$; $P < 0·01$). On average, the values of the inactivation time constant were 1·49-fold larger in BC than in PC patches over the range of membrane potentials investigated ($P < 0·05$ for 5 out of 10 potentials).

As the differences in inactivation time constant between the two types of neurones tended to be larger at more negative voltages (Fig. 4*C*), we extended the analysis to potentials that did not activate measurable Na^+ currents, using a protocol with prepulses of increasing duration (Fig. 5). The onset of inactivation of Na^+ channels at −55 mV was described by a single exponential function in both classes of neurones. The time constant was 18·6 ± 4·2 ms in BC patches ($n = 6$), whereas it was 9·3 ± 1·0 ms in PC patches ($n = 7$; $P < 0·05$; Fig. 5*C* and Table 1). These results show that the onset of inactivation is significantly slower for BC Na^+ channels than for PC Na^+ channels and that the difference becomes larger as the threshold potential for spike initiation is approached.

Recovery from inactivation

The time course of recovery of Na^+ channels from inactivation was investigated using double-pulse protocols,

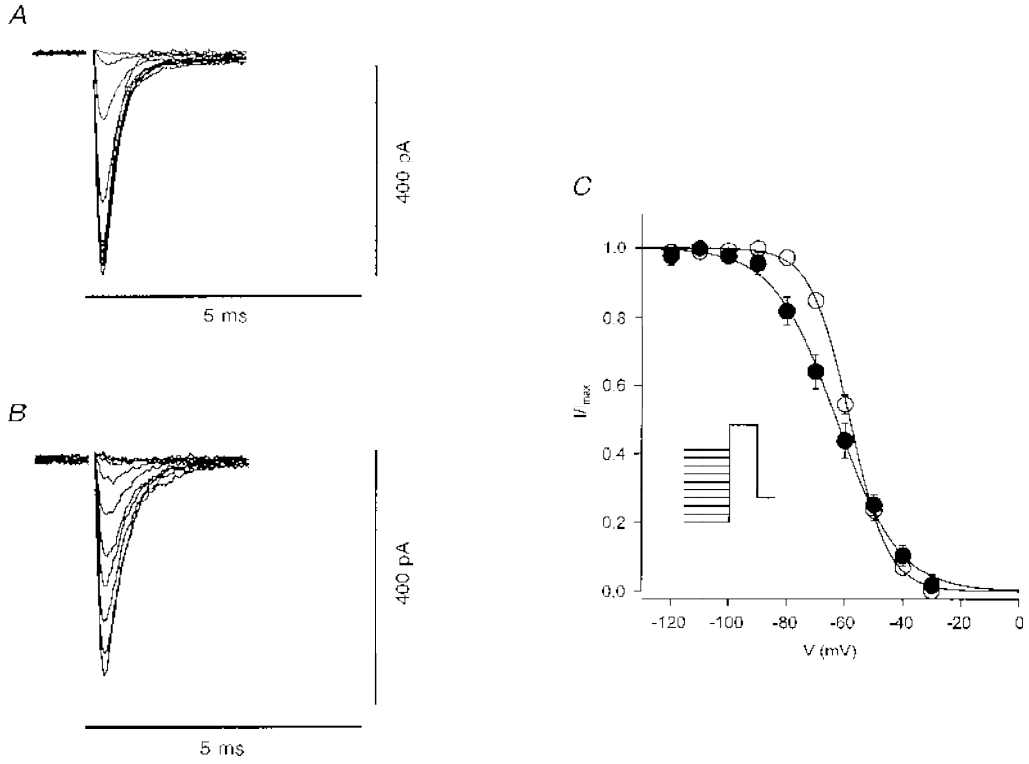

Figure 3. Voltage dependence of steady-state inactivation of Na^+ channels differs between BCs and PCs

A and *B*, steady-state inactivation in a BC nucleated patch (*A*) and a PC nucleated patch (*B*) induced by prepulses to different potentials. Pulse protocol: holding potential, −90 mV; 50 ms prepulse to voltages between −120 and −30 mV (10 mV increments); 30 ms test pulse to 0 mV; and step back to −90 mV (see inset in *C*). The internal solution was Cs^+-rich solution containing 4 mM Na^+. *C*, steady-state inactivation (h_∞) curve. Na^+ peak current amplitude, normalized to the maximal Na^+ current, was plotted against the prepulse potential. Open circles: mean values from 11 BC nucleated patches. Filled circles: mean values from 17 PC nucleated patches. Curves represent Boltzmann functions fitted to the data points; for curve parameters, see Table 1.

consisting of a pulse of either 30 or 300 ms duration to 0 mV that completely inactivated the channels, followed, at different time intervals, by a second pulse used to measure the extent of recovery from inactivation (Fig. 6). Na^+ channels in BC patches recovered completely from inactivation within less than 10 ms at −120 mV, independent of the duration of the conditioning pulse (Fig. 6*A* and *C*). The time course of recovery was mono-exponential; the time constant was 2·0 ms for the 30 ms conditioning pulse and 2·7 ms for the 300 ms pulse ($n = 13$ and $n = 3$, respectively; Fig. 6*C* and Table 1). In contrast, Na^+ channels in PCs did not recover completely from inactivation within 10 ms at this potential (Fig. 6*B*). The time course of recovery was bi-exponential; for 30 ms conditioning pulses the time constants were 2·0 and 133 ms, respectively, and the amplitude contribution of the slow component was 15% ($n = 8$–14; Fig. 6*D* and Table 1). For 300 ms conditioning pulses, the time constant of the fast component was almost identical (2·6 ms), but the time constant of the slow component was slower (351 ms) and its amplitude contribution increased to 24% ($n = 4$; $P < 0{\cdot}01$). Na^+ currents evoked by a series of nine pulses to 0 mV (30 ms duration), separated by pulses to −120 mV (12 ms duration), showed an almost constant amplitude in BC patches, but a decreasing amplitude in PC patches (Table 1). These results indicate that BC Na^+ channels recover from inactivation very rapidly, whereas PC Na^+ channels show a more complex time course of recovery that extends over hundreds of milliseconds.

DISCUSSION

To investigate voltage-gated Na^+ channels of neurones in rat brain slices, we used the nucleated patch configuration (Sather *et al.* 1992), which provides almost ideal voltage-clamp conditions and partly preserves the intracellular environment. We show that Na^+ channels expressed in GABAergic interneurones of the hippocampus differ from those in glutamatergic principal neurones in their functional properties. Whereas the differences in the activation process were confined to a faster deactivation time course of BC Na^+ channels at negative voltages, several differences were observed in the inactivation process. BC Na^+ channels differed from PC Na^+ channels in the shape of the steady-state inactivation curve, which was steeper and shifted to more positive potentials, and in the kinetics of inactivation, which showed a slower onset and a faster recovery.

The functional properties of Na^+ channels in CA1 pyramidal neurones, recorded in nucleated patches from rat brain slices

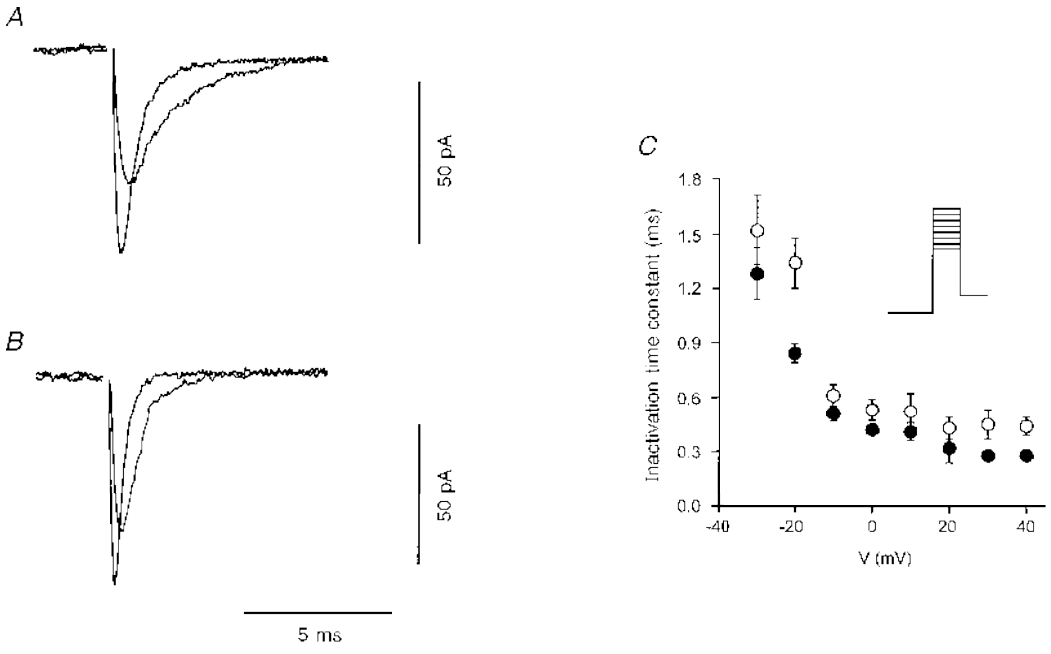

Figure 4. Time course of onset of inactivation at different membrane potentials in BC and PC patches

A and *B*, time course of onset of inactivation in a BC nucleated patch (*A*) and a PC nucleated patch (*B*) at −20 and 0 mV. Pulse protocol: holding potential, −90 mV; 50 ms pulse to −120 mV; 30 ms test pulse to −20 or 0 mV; and step back to −90 mV (see inset in *C*). The internal solution was Cs^+-rich solution containing 4 mM Na^+. *C*, inactivation time constant plotted against test pulse potential. Inactivation in all recordings was fitted by a single exponential. Open circles: mean values from 9–16 BC nucleated patches. Filled circles: mean values from 14–19 PC nucleated patches. Two PC patches that showed bi-exponential inactivation time courses at all potentials were not included in the plot.

(this paper) were considerably different from those reported previously for enzymatically dissociated neurones of the guinea-pig (Sah *et al.* 1988; French, Sah, Buckett & Gage, 1990). First, in the majority of dissociated CA1 neurones, inactivation was very slow (time constant of inactivation onset, 7·4 ms at −20 mV; 22–24 °C), while rapid inactivation comparable to that reported in the present study was found only in a subset of cells (time constant, 0·9 ms at −20 mV; Sah *et al.* 1988). Second, the mid-point potential of the steady-state inactivation curve was more negative in dissociated neurones ($V_{½} = -74{\cdot}9$ and $-67{\cdot}6$ mV for the slowly and the rapidly inactivating channels, respectively; Sah *et al.* 1988) than in nucleated patches from slices (this paper). Finally, a persistent TTX-sensitive Na^+ current (distinct from the window current generated by overlap of activation and inactivation curves) was reported in dissociated CA1 neurones (French *et al.* 1990; see Alzheimer, Schwindt & Crill, 1993), but was not detected in the present study. The reasons for these differences are not entirely clear. The absence of a persistent current component in nucleated patches is, however, consistent with previous estimates that its contribution to the total Na^+ current is small (< 1 %; Crill, 1996).

Diversity of Na^+ channels in the nervous system

Although the prevailing view is that voltage-gated Na^+ channels show less functional and molecular diversity than other types of ion channels (e.g. K^+ channels; Jonas, Bräu, Hermsteiner & Vogel, 1989), differences in the voltage dependence and time course of inactivation of Na^+ channels between different types of neurones have been described previously. In motor myelinated nerve fibres the onset of inactivation is relatively slow and bi-exponential, whereas in sensory fibres it is faster and well approximated by a single exponential function (Schwarz, Bromm, Spielmann & Weytjens, 1983). It was suggested that these distinct properties of Na^+ channels may contribute to the characteristic shape of action potentials in motor and sensory fibres (reviewed by Vogel & Schwarz, 1995).

Differences in Na^+ channel inactivation properties between BCs and PCs of the hippocampus resemble those between dorsal ganglion neurones and motor neurones of the spinal cord reported previously (Ogata & Tatebayashi, 1993; Safronov & Vogel, 1995). In sensory neurones of dorsal root ganglia, TTX-sensitive Na^+ channels recover from inactivation very rapidly (time constant, 5 ms at −100 mV)

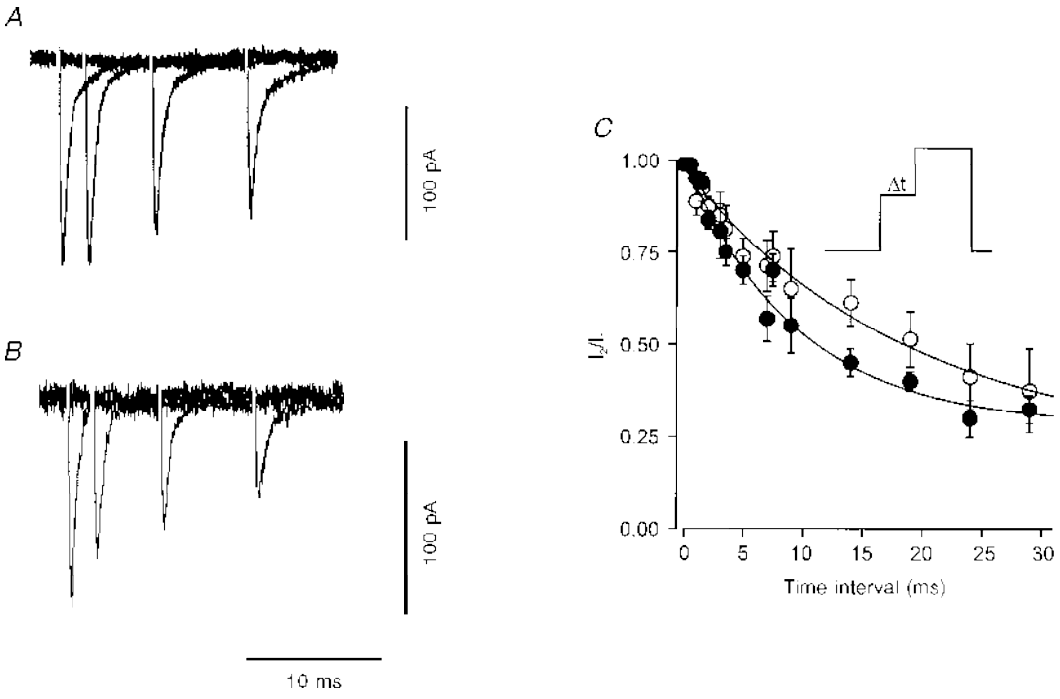

Figure 5. Time course of onset of inactivation of Na^+ channels at subthreshold membrane potentials differs between BCs and PCs

A and *B*, time course of onset of inactivation in a BC nucleated patch (*A*) and a PC nucleated patch (*B*) at −55 mV. Pulse protocol: holding potential, −90 mV; 50 ms pulse to −120 mV; prepulse to −55 mV of variable duration; 30 ms test pulse to 0 mV; and step back to −90 mV (see inset in *C*). First traces on the left represent Na^+ currents without prepulses ($\Delta t = 0$). The internal solution was Cs^+-rich solution containing 4 mM Na^+. *C*, Na^+ peak current amplitude, normalized to a response evoked by a test pulse without prepulse, was plotted against prepulse duration. Open circles: mean values from 6 BC nucleated patches. Filled circles: mean values from 7 PC nucleated patches. Curves represent exponential functions fitted to the data points; the final values reached by the curves for long time intervals were constrained to the values of h_∞ at −55 mV (Fig. 3). For time constants, see Table 1.

and the voltage dependence of steady-state inactivation is steep (slope factor, 5·2 mV; Ogata & Tatebayashi, 1993), as found for BCs. In contrast, Na^+ channels in motor neurones show a slower recovery from inactivation (time constants, 16 and 153 ms at −80 mV) and a less steep steady-state inactivation curve (slope factor, 10·2 mV; Safronov & Vogel, 1995), similar to those in PCs. It was suggested that these differences may contribute to the higher limiting action potential frequency in sensory in comparison to motor neurones (Safronov & Vogel, 1995).

The molecular basis of the differences in Na^+ channel gating in BCs and PCs remains unclear. Voltage-gated Na^+ channels expressed in the CNS are heteromers composed of principal α-subunits (α_1–α_3, reviewed by Catterall, 1992; NaG, Gautron, Dos Santos, Pinto-Henrique, Koulakoff, Gros & Berwald-Netter, 1992; Na6, Schaller, Krzemien, Yarowsky, Krueger & Caldwell, 1995) and auxiliary β-subunits (β_1, β_2; reviewed by Catterall, 1992). Recombinant channels assembled from α_2-subunits show faster gating than those formed by α_3-subunits (Joho *et al.* 1990) and channels containing the β_1-subunit show faster inactivation onset and recovery than those lacking the β_1-subunit (Isom *et al.* 1992; Makita, Bennett & George, 1996). This suggests that differential subunit expression in BCs and PCs may account for the functional differences observed. Alternatively, Na^+ channel gating could be affected by differential modulation. Since Ca^{2+}-dependent phosphorylation by protein kinase C slows the onset of Na^+ channel inactivation (Cantrell, Ma, Scheuer & Catterall, 1996), a differential modulation of Na^+

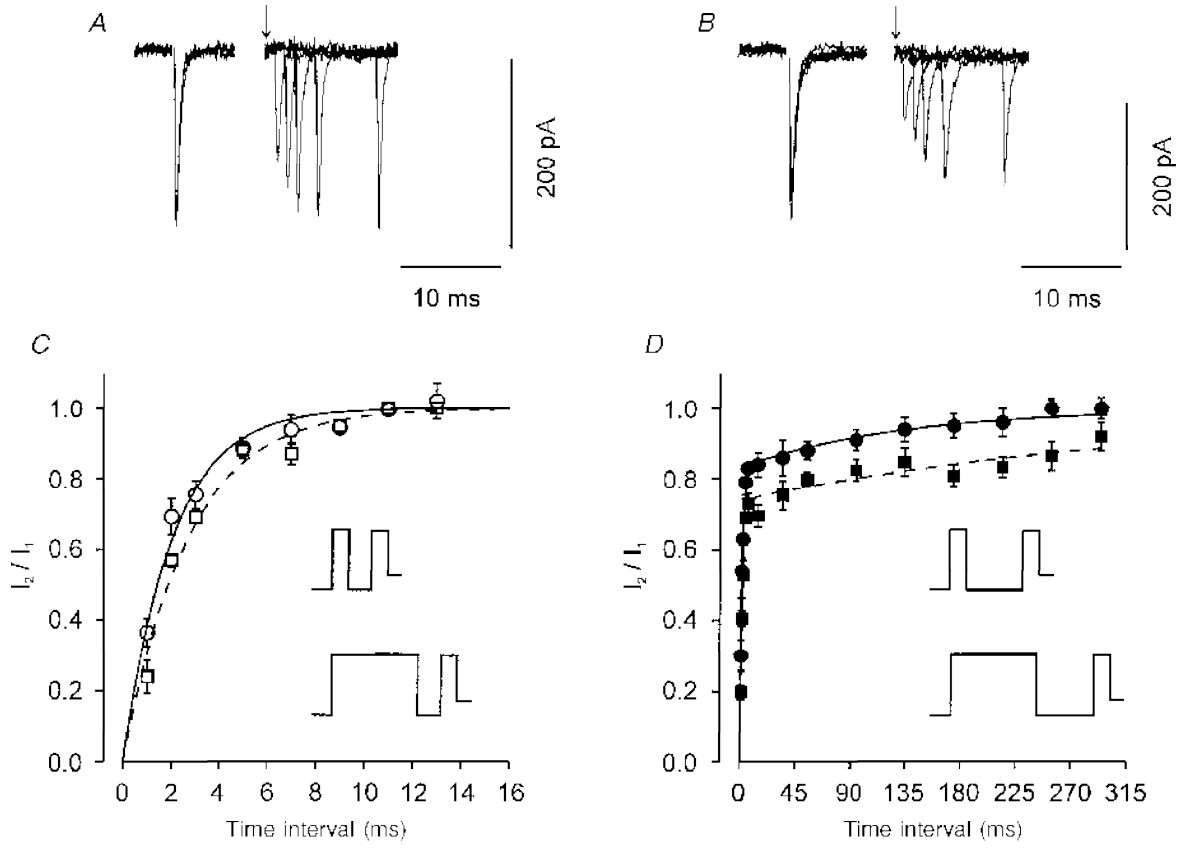

Figure 6. Time course of recovery of Na^+ channels from inactivation differs between BCs and PCs

A and *B*, recovery from inactivation in a BC nucleated patch (*A*) and a PC nucleated patch (*B*). Pulse protocol: holding potential, −90 mV; 50 ms pulse to −120 mV; 30 ms pulse to 0 mV (conditioning pulse); pulse of variable duration to −120 mV; 30 ms pulse to 0 mV (test pulse); and step back to −90 mV (see inset in *C* and *D*). Responses to the conditioning pulse are shown on the left, responses to the test pulse on the right; arrow indicates the end of the conditioning pulse. The internal solution was Cs^+-rich solution containing 4 mM Na^+. *C* and *D*, ratio of peak amplitude of the Na^+ current evoked by the test pulse to that evoked by the conditioning pulse, plotted against the duration of the interpulse interval. Curves represent either single exponential functions (for BC channels) or sums of two exponentials (for PC channels) fitted to the data points. Circles and continuous curves, 30 ms conditioning pulse, data points represent mean values from 13 BC nucleated patches (*C*) and 8–14 PC nucleated patches (*D*). Squares and dashed curves, 300 ms conditioning pulse, data points represent mean values from 3 BC nucleated patches (*C*) and 4–7 PC nucleated patches (*D*). For curve parameters, see Table 1.

channels in principal neurones and interneurones is perhaps compatible with the specific expression of Ca^{2+}-permeable AMPA-type glutamate receptors in GABAergic interneurones (reviewed by Jonas & Burnashev, 1995).

Possible impact of differences in Na^+ channel gating on the action potential pattern

The diverse action potential patterns of cortical neurones (reviewed by Connors & Gutnick, 1990) are determined by the interplay between voltage-gated Na^+ and K^+ channels in combination with morphological properties and channel distribution along the somatodendritic axis (Mainen & Sejnowski, 1996). Previous studies suggested that these differences in spiking patterns were largely determined by the expression of different K^+ channels. Fast-spiking interneurones in the stratum oriens–alveus and pyramidale of the CA1 region of the hippocampus express voltage-gated K^+ channels that activate and deactivate very rapidly, but inactivate only very slowly (Zhang & McBain, 1995*a*, *b*; Du, Zhang, Weiser, Rudy & McBain, 1996). These specific properties of interneurone K^+ channels ensure the rapid repolarization of action potentials that is required for fast spiking.

The present results reveal a more complex picture, and suggest that the functional properties of voltage-gated Na^+ channels contribute to the differences in action potential pattern. (1) The difference in steepness of the steady-state inactivation curve between Na^+ channels in BCs and those in PCs generates a different overlap of inactivation and activation curves. Increased overlap between inactivation and activation curves could augment the amplitude of the slow depolarizing potential during repetitive spiking, and thus may facilitate intrinsic bursting in CA1 pyramidal neurones (Warman, Durand & Yuen, 1994; M. Martina & P. Jonas, unpublished simulations). (2) The difference in recovery from inactivation regulates the fraction of available Na^+ channels during a spike train. Fast recovery of BC Na^+ channels supports fast spiking, whereas slow recovery of PC Na^+ channels leads to adaptation (Fleidervish *et al.* 1996). Unlike in neocortical neurones (Fleidervish *et al.* 1996), a single brief depolarizing pulse was sufficient to induce prolonged inactivation in hippocampal PCs; a long pulse or a train of multiple pulses was, however, more effective and induced cumulative prolonged inactivation. Thus PC Na^+ channels could enter long-lived inactivated states following a few action potentials or even a single spike.

The differences in recovery of Na^+ channels from inactivation between principal neurones and interneurones of the hippocampus may shape the transformation of synaptic input signals into action potential output signals. BC-type Na^+ channels could facilitate the generation of trains of action potentials that retain the precise temporal structure of synaptic input. The fast recovery of BC-type Na^+ channels from inactivation could also enable interneurones to fire spike doublets that may synchronize spatially distributed principal neurone ensembles (Traub, Whittington, Stanford & Jefferys, 1996). By contrast, the slow recovery of PC-type Na^+ channels from inactivation may enable PCs to differentiate synaptic input, because only a few action potentials are generated in response to repetitive synaptic stimulation.

If Na^+ channels in the dendrites are functionally similar to those in the soma, the present results may imply distinct forms of action potential backpropagation into the dendrites of different types of cortical neurones. BC-type Na^+ channels with fast recovery from inactivation could facilitate the reliable backpropagation of action potential trains into interneurone dendrites (reviewed by Johnston, Magee, Colbert & Christie, 1996). Conversely, the expression of PC-type Na^+ channels with slow recovery perhaps explains why in CA1 pyramidal neurones spikes occurring early in a train propagate actively, whereas those occurring later fail to actively invade the dendrites (Spruston, Schiller, Stuart & Sakmann, 1995).

Alzheimer, C., Schwindt, P. C. & Crill, W. E. (1993). Modal gating of Na^+ channels as a mechanism of persistent Na^+ current in pyramidal neurons from rat and cat sensorimotor cortex. *Journal of Neuroscience* **13**, 660–673.

Cantrell, A. R., Ma, J. Y., Scheuer, T. & Catterall, W. A. (1996). Muscarinic modulation of sodium current by activation of protein kinase C in rat hippocampal neurons. *Neuron* **16**, 1019–1026.

Catterall, W. A. (1992). Cellular and molecular biology of voltage-gated sodium channels. *Physiological Reviews* **72**, S15–48.

Colquhoun, D. & Sigworth, F. J. (1995). Fitting and statistical analysis of single-channel records. In *Single-Channel Recording*, ed. Sakmann, B. & Neher, E., pp. 483–587. Plenum Press, New York.

Connors, B. W. & Gutnick, M. J. (1990). Intrinsic firing patterns of diverse neocortical neurons. *Trends in Neurosciences* **13**, 99–104.

Crill, W. E. (1996). Persistent sodium current in mammalian central neurons. *Annual Review of Physiology* **58**, 349–362.

Du, J., Zhang, L., Weiser, M., Rudy, B. & McBain, C. J. (1996). Developmental expression and functional characterization of the potassium-channel subunit Kv3.1b in parvalbumin-containing interneurons of the rat hippocampus. *Journal of Neuroscience* **16**, 506–518.

Fleidervish, I. A., Friedman, A. & Gutnick, M. J. (1996). Slow inactivation of Na^+ current and slow cumulative spike adaptation in mouse and guinea-pig neocortical neurones in slices. *Journal of Physiology* **493**, 83–97.

French, C. R., Sah, P., Buckett, K. J. & Gage, P. W. (1990). A voltage-dependent persistent Na^+ current in mammalian hippocampal neurons. *Journal of General Physiology* **95**, 1139–1157.

Gautron, S., Dos Santos, G., Pinto-Henrique, D., Koulakoff, A., Gros, F. & Berwald-Netter, Y. (1992). The glial voltage-gated sodium channel: Cell- and tissue-specific mRNA expression. *Proceedings of the National Academy of Sciences of the USA* **89**, 7272–7276.

Han, Z.-S., Buhl, E. H., Lörinczi, Z. & Somogyi, P. (1993). A high degree of spatial selectivity in the axonal and dendritic domains of physiologically identified local-circuit neurons in the dentate gyrus of the rat hippocampus. *European Journal of Neuroscience* **5**, 395–410.

Hille, B. (1992). *Ionic channels of excitable membranes.* Sinauer Associates, Sunderland, MA, USA.

Howe, J. R. & Ritchie, J. M. (1992). Multiple kinetic components of sodium channel inactivation in rabbit Schwann cells. *Journal of Physiology* **455**, 529–566.

Isom, L. L., De Jongh, K. S., Patton, D. E., Reber, B. F. X., Offord, J., Charbonneau, H., Walsh, K., Goldin, A. L. & Catterall, W. A. (1992). Primary structure and functional expression of the β_1 subunit of the rat brain sodium channel. *Science* **256**, 839–842.

Johnston, D., Magee, J. C., Colbert, C. M. & Christie, B. R. (1996). Active properties of neuronal dendrites. *Annual Review of Neuroscience* **19**, 165–186.

Joho, R. H., Moorman, J. R., VanDongen, A. M. J., Kirsch, G. E., Silberberg, H., Schuster, G. & Brown, A. M. (1990). Toxin and kinetic profile of rat brain type III sodium channels expressed in *Xenopus* oocytes. *Molecular Brain Research* **7**, 105–113.

Jonas, P. (1989). Temperature dependence of gating current in myelinated nerve fibers. *Journal of Membrane Biology* **112**, 277–289.

Jonas, P., Bräu, M. E., Hermsteiner, M. & Vogel, W. (1989). Single-channel recording in myelinated nerve fibers reveals one type of Na channel but different K channels. *Proceedings of the National Academy of Sciences of the USA* **86**, 7238–7242.

Jonas, P. & Burnashev, N. (1995). Molecular mechanisms controlling calcium entry through AMPA-type glutamate receptor channels. *Neuron* **15**, 987–990.

Lacaille, J.-C. & Williams, S. (1990). Membrane properties of interneurons in stratum oriens-alveus of the CA1 region of rat hippocampus *in vitro*. *Neuroscience* **36**, 349–359.

McCormick, D. A., Connors, B. W., Lighthall, J. W. & Prince, D. A. (1985). Comparative electrophysiology of pyramidal and sparsely spiny stellate neurons of the neocortex. *Journal of Neurophysiology* **54**, 782–802.

Madison, D. V. & Nicoll, R. A. (1984). Control of the repetitive discharge of rat CA1 pyramidal neurones *in vitro*. *Journal of Physiology* **354**, 319–331.

Mainen, Z. F. & Sejnowski, T. J. (1996). Influence of dendritic structure on firing pattern in model neocortical neurons. *Nature* **382**, 363–366.

Makita, N., Bennett, P. B. & George, A. L. Jr (1996). Molecular determinants of β_1 subunit-induced gating modulation in voltage-dependent Na^+ channels. *Journal of Neuroscience* **16**, 7117–7127.

Ogata, N. & Tatebayashi, H. (1993). Kinetic analysis of two types of Na^+ channels in rat dorsal root ganglia. *Journal of Physiology* **466**, 9–37.

Safronov, B. V. & Vogel, W. (1995). Single voltage-activated Na^+ and K^+ channels in the somata of rat motoneurones. *Journal of Physiology* **487**, 91–106.

Sah, P., Gibb, A. J. & Gage, P. W. (1988). The sodium current underlying action potentials in guinea pig hippocampal CA1 neurons. *Journal of General Physiology* **91**, 373–398.

Sather, W., Dieudonné, S., MacDonald, J. F. & Ascher, P. (1992). Activation and desensitization of *N*-methyl-D-aspartate receptors in nucleated outside-out patches from mouse neurones. *Journal of Physiology* **450**, 643–672.

Schaller, K. L., Krzemien, D. M., Yarowsky, P. J., Krueger, B. K. & Caldwell, J. H. (1995). A novel, abundant sodium channel expressed in neurons and glia. *Journal of Neuroscience* **15**, 3231–3242.

Schwarz, J. R., Bromm, B., Spielmann, R. P. & Weytjens, J. L. F. (1983). Development of Na inactivation in motor and sensory myelinated nerve fibres of *Rana esculenta*. *Pflügers Archiv* **398**, 126–129.

Spruston, N., Schiller, Y., Stuart, G. & Sakmann, B. (1995). Activity-dependent action potential invasion and calcium influx into hippocampal CA1 dendrites. *Science* **268**, 297–300.

Stafstrom, C. E., Schwindt, P. C. & Crill, W. E. (1984). Repetitive firing in layer V neurons from cat neocortex in vitro. *Journal of Neurophysiology* **52**, 264–277.

Storm, J. F. (1990). Potassium currents in hippocampal pyramidal cells. *Progress in Brain Research* **83**, 161–187.

Stuart, G. J., Dodt, H.-U. & Sakmann, B. (1993). Patch-clamp recordings from the soma and dendrites of neurons in brain slices using infrared video microscopy. *Pflügers Archiv* **423**, 511–518.

Terlau, H., Shon, K.-J., Grilley, M., Stocker, M., Stühmer, W. & Olivera, B. M. (1996). Strategy for rapid immobilization of prey by a fish-hunting marine snail. *Nature* **381**, 148–151.

Traub, R. D., Whittington, M. A., Stanford, I. M. & Jefferys, J. G. R. (1996). A mechanism for generation of long-range synchronous fast oscillations in the cortex. *Nature* **383**, 621–624.

Vogel, W. & Schwarz, J. R. (1995). Voltage-clamp studies in axons: Macroscopic and single-channel currents. In *The Axon*, ed. Waxman, S. G., Kocsis, J. D. & Stys, P. K., pp. 257–280. Oxford University Press, Oxford.

Warman, E. N., Durand, D. M. & Yuen, G. L. F. (1994). Reconstruction of hippocampal CA1 pyramidal cell electrophysiology by computer simulation. *Journal of Neurophysiology* **71**, 2033–2045.

Zhang, L. & McBain, C. J. (1995*a*). Voltage-gated potassium currents in stratum oriens–alveus inhibitory neurones of the rat CA1 hippocampus. *Journal of Physiology* **488**, 647–660.

Zhang, L. & McBain, C. J. (1995*b*). Potassium conductances underlying repolarization and after-hyperpolarization in rat CA1 hippocampal interneurones. *Journal of Physiology* **488**, 661–672.

Acknowledgements

We thank Drs J. Bischofberger and J. R. P. Geiger for critically reading the manuscript, Mrs B. Plessow-Freudenberg and K. Zipfel for technical assistance, and Mrs B. Hillers for typing. This work was supported by the German Israeli Foundation grant I 0352-073.01/94 to P.J.

Author's email address

P. Jonas: jonasp@ruf.uni-freiburg.de

Received 22 April 1997; accepted 8 August 1997.